Research Square

Preprints are preliminary reports that have not undergone peer review.
They should not be considered conclusive, used to inform clinical practice,
or referenced by the media as validated information.

In silico Discovery of Novel Antibacterial Compounds against Staphylococcus aureus Targeting Extracellular Domain of Lipoteichoic Acid Synthase, Quantum mechanical quantification, and in vitro experimental validation

Seiya Morita
Kyushu Institute of Technology
Mikuri Yokota
Kyushu Institute of Technology
Kotomi Saiki
Kyushu Institute of Technology
Subaru Shioi
Kyushu Institute of Technology
Shunsuke Aoki
shuaokis@aokislab.com

Kyushu Institute of Technology

Research Article

Keywords: staphylococcus aureus, in silico screening, lipoteichoic acid synthase, molecular dynamics simulation, Ab initio fragment molecular orbital method

Posted Date: March 2nd, 2026

DOI: https://doi.org/10.21203/rs.3.rs-8922369/v1

License: This work is licensed under a Creative Commons Attribution 4.0 International License.
Read Full License

Additional Declarations: No competing interests reported.

Abstract

Staphylococcus aureus is a major causative agent of serious hospital-acquired infections, including pneumonia and sepsis. The emergence of drug-resistant strains such as methicillin-resistant and vancomycin-resistant *S. aureus* poses a global threat. Infections caused by these multidrug-resistant bacteria are predicted to become a leading cause of human mortality in the future. However, the development pipeline for new antibiotics is declining, raising concerns about a future shortage of effective treatments. Therefore, the discovery of novel antimicrobial agents, particularly those with new mechanisms of action, is urgently needed. In this study, we aimed to discover novel antimicrobial compounds by targeting Lipoteichoic acid synthase (LtaS). LtaS is a membrane protein essential for the synthesis of lipoteichoic acid (LTA), a key cell wall component in *S. aureus*. We performed a hierarchical *in silico* screening of the ChemBridge chemical 3D structure library, which contains about 150 thousand compounds. The screening identified a compound (7195703) as a promising lead candidate. Quantum mechanical calculation of DG using the FMO method yielded a value of -93.64 kcal/mol. To evaluate its antimicrobial activity, an *in vitro* growth inhibition assay was performed using *Staphylococcus epidermidis*, a closely related model organism for *S. aureus*. 7195703 exhibited potent and dose-dependent growth inhibition against *S. epidermidis*, with a half-maximal inhibitory concentration (IC_{50}) of 16.61 μM. Conversely, 7195703 showed no significant inhibitory activity against the Gram-negative bacterium *Escherichia coli*, suggesting its selective activity against certain Gram-positive bacteria. Furthermore, a search for structural analogues of 7195703 identified five derivatives that also displayed antimicrobial activity.

1. Introduction

Staphylococcus aureus (*S. aureus*), a Gram-positive commensal bacterium found on human skin and in the nasal passages, is an opportunistic pathogen that causes severe infections, including pneumonia and sepsis, particularly in immunocompromised hosts[1, 2]. The treatment of *S. aureus* infectious diseases is further complicated by the emergence of multidrug-resistant strains, notably methicillin-resistant *S. aureus* (MRSA) and vancomycin-resistant *S. aureus* (VRSA)[3]. In addition to conventional hospital-acquired MRSA (HA-MRSA), community-acquired MRSA (CA-MRSA) has now emerged, posing a new clinical threat due to its ability to infect even healthy young populations. CA-MRSA produces Panton-Valentine leucocidin (PVL), a cytotoxin that causes severe necrotizing pneumonia associated with a high mortality rate[4, 5]. Despite the emergence of highly threatening drug-resistant bacteria, the number of newly approved antimicrobial agents continues to decline, raising concerns about the future depletion of effective treatments. To address the future challenge of antimicrobial depletion, large-scale *in silico* screening is considered an effective strategy for the discovery of new antimicrobial drugs[6].

LtaS is a polytopic membrane protein involved in the cell wall synthesis of Gram-positive bacteria, such as *S. aureus*. LtaS possesses five transmembrane domains and a large extracellular catalytic domain (eLtaS) that functions on the outer surface of the bacterial membrane. LtaS synthesizes polyglycerol-phosphate (type I) lipoteichoic acid (LTA) by using phosphatidylglycerol (PG) as a substrate and

sequentially adds glycerol-phosphate units to the Glc_2-DAG anchor. Type I LTA is a crucial component of the bacterial cell wall. LtaS plays an essential role in the survival and proliferation of *S. aureus*. It mediates the adsorption of magnesium ions (Mg^{2+}) due to the negative charge of LTA and the localization of cell wall degradation enzymes triggered by pH changes. LtaS-deficient mutants exhibit growth abnormalities, leading to the identification of LtaS as a potential drug target in *S. aureus* [7, 8]. Inhibitory compounds targeting eLtaS offer a significant advantage in drug discovery because they do not need to cross the cell membrane [9]. The X-ray crystal structure of eLtaS has been determined (Fig. 1).

Structure-based drug screening (SBDS) is a computational method for discovering drugs that bind to the active site structure of target proteins. SBDS rapidly screens vast numbers of compounds, reducing time and cost in drug discovery. Several cases of novel antimicrobial compound identification via SBDS have been reported [11, 12]. Docking simulation tools such as DOCK [13], GOLD [14], AutoDock Vina (ADV) [15], and GNINA [16]are used in SBDS. Hierarchical *in silico* SBDS combining multiple tools is a powerful approach for efficiently identifying drugs.

In this study, a novel antimicrobial lead compound, 7195703, was identified through a hierarchical *in silico* SBDS approach combining GNINA docking and molecular dynamics simulations targeting *S. aureus* eLtaS. 7195703 exhibited antimicrobial activity (IC_{50} = 16.61 μM) against *Staphylococcus epidermidis* (*S. epidermidis*). However, it showed no antimicrobial effect against Gram-negative bacteria. These data suggest that 7195703 possesses high potential as a lead compound for future anti-bacterial drug development.

2. Methods

2.1 Compound Data Library

This study utilized a three-dimensional chemical structure library containing 154,118 compounds provided by ChemBridge. This library was obtained from the web-based database of the Ressource Parisienne en Bioinformatique Structurale (https://chembridge.com/). The library has been pre-filtered using ADME/Tox criteria to exclude compounds with properties unsuitable for drug development. For the analogue search of the hit compound, a library comprising 1,638,575 compounds from ChemBridge was utilized (https://chembridge.com/). This library incorporates the company's "CORE Library Stock," which consists of small molecules exhibiting lead-like properties. These compounds were virtually assessed before synthesis to ensure that only those with favorable physicochemical profiles and free from undesirable chemical functionalities were selected.

2.2 GNINA

GNINA is an AI-based molecular docking software that employs a scoring function based on a convolutional neural network (CNN), which has been trained and tested on the PDBbind database. It generates features by mapping 14 distinct ligand atom types and 14 receptor atom types onto a 0.5 Å

resolution cubic grid. These features are then used to predict both the binding affinity and the quality of the binding pose (CNN score) for a given protein-ligand complex. GNINA was used for the first step screening using the three-dimensional chemical structure library of 154,118 compounds from ChemBridge.

2.3 Preparation of Target Protein

The X-ray crystal structure of *S. aureus* eLtaS (PDB ID: 2W5Q) was obtained from the Protein Data Bank. The structure, resolved at 1.20 Å, provided a resolution sufficient for the subsequent hierarchical *in silico* SBDS. The protein structure was preprocessed using the Molecular Operating Environment (MOE). This preparation included the addition of hydrogen atoms using the Protonate 3D module (MMFF94x force field), calculation of partial charges with the Partial Charge module, and energy minimization of the structure with the Energy Minimize module.

2.4 Molecular Dynamics simulation (MDS)

We simulated the dynamic behavior, intermolecular interactions, and structural changes of the docked protein-ligand complex using MDS and evaluated the binding stability of the complex classically. The simulation system was prepared using the Solution Builder within CHARMM-GUI[17, 18] with the CHARMM36m force field. Each complex was placed in a cubic water box using the TIP3P water model and buffered in 0.15 M NaCl. Short-range electrostatic and van der Waals interactions were simulated using the Verlet method with a 12 Å cutoff, while long-range electrostatic interactions were handled by the particle mesh Ewald (PME) method. All bonds involving hydrogen atoms were constrained using the LINCS algorithm[19]. The systems, each containing approximately 30,000 atoms, were first energy-minimized for up to 5,000 steps with the steepest descent method. Subsequently, the systems were equilibrated in two 100 ps stages: first in the NVT ensemble (310 K) and then in the NPT ensemble (310 K, 1 bar). All simulations were conducted using GROMACS 2022.4.

2.5 Trajectory Analysis

The stability of the protein-ligand complex was evaluated by calculating the root mean square deviation of the ligand (ligand RMSD) relative to backbone atoms in the protein structure. Ligand RMSD quantifies the deviation of the ligand's binding pose from the initial docking structure throughout the simulation and can be used to evaluate binding stability.

2.6 MM-GBSA method

To estimate the binding free energy of the protein-ligand complex, we employed the molecular mechanics generalized Born surface area (MM-GBSA) method. The calculations were performed using the gmx_MMPBSA tool on the trajectories obtained from the GROMACS 2022.4 simulations.

2.7 *Ab initio* fragment molecular orbital (FMO) method

The FMO method is a technique for performing first-principles quantum mechanical calculations at high speed by dividing large molecular systems into fragments and solving the Schrödinger equation in parallel for each fragment[20, 21]. It was implemented using the ABINIT-MP software package[22]. The electronic states of each fragment were calculated using the MP2/6-31G basis set to determine the total electron density of the entire system[23]. The binding free energy of the protein-ligand complex was quantitatively analyzed using $IFIE_{total}$, obtained by summing the inter-fragment interaction energy (IFIE) between the ligand and all amino acid residues of the protein[24].

2.8 Growth inhibitory assay against *S. epidermidis*

An antimicrobial activity test was conducted using *Staphylococcus epidermidis* to verify the antibacterial activity of the selected compound. *S. epidermidis* was used as a surrogate for *S. aureus* because *S. aureus* is a biosafety level 2 pathogen. The amino acid sequence identity between *S. aureus* eLtaS and *S. epidermidis* eLtaS was 88 % as analyzed by the BLAST server. 7195703 was purchased from ChemBridge and dissolved in dimethyl sulfoxide (DMSO, Sigma) to a concentration of 33 mM. *S. epidermidis* was obtained from the RIKEN BioResource Research Center (Saitama, Japan). An aliquot of the *S. epidermidis* stock culture was added to the culture medium [1 % peptone (BD), 1 % meat extract (BD), 0.5 % NaCl (Wako, Japan), pH 7.0] to a final concentration of 25 % (v/v), and cultured at 37 °C and 240 rpm for 2 h. The culture was then diluted 20-fold with the medium. We added 7195703, or ampicillin (positive control), to a final concentration of 100 mM, and DMSO (negative control) to a final concentration of 0.3 %. This mixture was dispensed at 200 mL per well into a 96-well plate, incubated at 37 °C and 240 rpm for 3.5 h, and the turbidity (OD^{590}) was measured using an MPR-A100 microplate reader (AS ONE).

2.9 Growth inhibitory assay against *Escherichia coli* (*E. coli*)

To investigate the antibacterial spectrum of the selected compound, we performed growth inhibitory assays using *E. coli*. The *E. coli* BL21 strain stock solution was added to Luria-Bertani (LB) medium [1 % Bacto Tryptone (BD), 0.5 % Yeast Extract (BD), 1 % NaCl (Wako, Japan), pH 7.0] to a final concentration of 25 % (v/v) and cultured at 37 °C and 204 rpm for 3 h. The culture was then diluted 20-fold with the medium. We added 7195703, or ampicillin (positive control), to a final concentration of 100 mM, and DMSO (negative control) to a final concentration of 0.3 %. This mixture was dispensed at 200 mL per well into a 96-well plate, incubated at 37 °C and 204 rpm for 8 h, and the turbidity (OD^{590}) was measured using an MPR-A100 microplate reader (AS ONE).

2.10 Toxicity Assay against Mammalian Cells

For toxicity testing of 7195703, we used African green monkey kidney-derived COS-7 cells and human liver-derived HepG2 cells. The number of viable cells was measured using the Cell Counting Kit-8. Each cell line was seeded in 100 mm dishes and cultured in D-MEM medium [10 % FBS, 1 % non-essential amino acids, 1 % L-Glutamine, 1 % Penicillin-Streptomycin, pH 7.0] at 37 °C under 5 % CO2 conditions. The cells were then seeded into 96-well plates at a density of 1.0×10^4 cells/well. After culturing for 6 h, the medium was replaced with D-MEM starvation medium [0.25 % FBS, 1 % L-Glutamine, 1 % Penicillin-

Streptomycin, pH 7.0]. The cells were further cultured overnight at 37 °C under 5 % CO2 conditions. The medium was replaced with starvation medium containing 7195703 and cultured overnight. Subsequently, Cell Counting Kit-8 solution was added to each well, and after 2 h, the absorbance was measured at 405 nm using an MPR-A100 microplate reader (AS ONE).

2.11 Drug-Likeness Analysis and Toxicity Prediction

The toxicity profiles of the selected compounds were predicted *in silico* using two web-based tools: SwissADME and ProTox-3.0. The SwissADME server was utilized to estimate absorption, distribution, metabolism, and excretion (ADME) parameters, as well as other pharmacokinetic properties[25]. The ProTox-3.0 server predicted various toxicological endpoints, including cytotoxicity and carcinogenicity[26, 27].

2.12 Statistical Analysis

All data were statistically analyzed using GraphPad Prism version 4 (GraphPad Software, Inc., San Diego, CA, USA).

2.13 Declaration of generative AI and AI-assisted technologies in the manuscript preparation process

During the preparation of this work the authors used DeepL and Gemini in order to improve the readability and ensure the grammatical accuracy of the manuscript. After using these tools/services, the authors reviewed and edited the content as needed and take full responsibility for the content of the published article.

3. Results

3.1 Hierarchical *in silico* SBDS

Hierarchical *in silico* SBDS targeting *S. aureus* eLtaS was performed using the ChemBridge 3D structure library of 154,118 compounds (**Fig. 2**). In the primary screening, docking simulations with GNINA were conducted, selecting the top 10 compounds based on CNN affinity and CNN score, respectively, for a total of 20 compounds. In the secondary screening, MDS was performed for 10 ns using their docking poses as initial structures, resulting in the selection of 8 compounds with a maximum ligand RMSD value of less than 0.55 nm (**Fig. S1** in Online Resource 1). In the tertiary screening, MDS was applied to these 8 compounds for 50 ns, and the 6 compounds with average ligand RMSD values below 0.55 nm were then analyzed with MM-GBSA (**Fig. S2** in Online Resource 1). From this analysis, two compounds with negative maximum DG values were selected (**Table S1** in Online Resource 1). Finally, these two compounds underwent two additional 50 ns MDS runs, and the compound that maintained an average ligand RMSD value below 0.55 nm in all three simulations was designated as the final hit compound (**Table S2**, **Fig. S3** in Online Resource 1). The structure of the final hit compound is shown in **Table S3** and **Fig. S4** in Online Resource 1.

3.2 Growth inhibitory assay against *S. epidermidis*

The growth inhibition assay against *S. epidermidis* showed that 7195703 significantly inhibited the growth of *S. epidermidis* (**Fig. 3**). The growth inhibition rate was 83.52%. The dose-dependent effect of 7195703 on *S. epidermidis* was also analyzed, and the 50% growth inhibition concentration (IC_{50} value) was found to be 16.61 mM (**Fig. 4**).

3.3 Analysis of the Binding Mode and Interaction Energy of *S. aureus* eLtaS-7195703

The binding mode of *S. aureus* eLtaS and 7195703 was analyzed using the Protein-Ligand Interaction Profiler (PLIP). 7195703 was predicted to form hydrophobic interactions with TRP354, LEU384, and LEU413, and hydrogen bonds with TRP354 and ARG356 (**Fig. 5**). Inter-fragment interaction energy analysis was performed using *ab initio* FMO calculations, and the total IFIE between *S. aureus* eLtaS and 7195703 was -93.64 kcal/mol. The top three residues for IFIE, as calculated by the FMO analysis, were ASP349, ARG356, and TRP354 (**Table 1**). Among these, ARG356 is predicted to form a hydrogen bond with the previously identified inhibitor Compound 1771[28], reaffirming its importance in inhibiting the LTA production of LtaS.

Table 1: Top 3 residues with the highest FMO IEIE values

amino acid residue	IFIE (kcal/mol)
ASP349	-35.66
ARG356	-24.84
TRP354	-12.48

3.4 Growth inhibitory assay against *E. coli*

A growth inhibition assay of 7195703 against *E. coli* was performed. The results showed that 7195703 did not inhibit the growth of *E. coli* (**Fig. 6**). This result suggests that 7195703 selectively inhibits the growth of *S. epidermidis*.

3.5 Toxicity Assay against Mammalian Cells

Cytotoxicity assays for 7195703 were conducted using human liver-derived HepG2 cells and African green monkey kidney-derived COS-7 cells. 7195703 exhibited a 19.71% growth inhibitory effect against HepG2 cells (**Fig. 7A**), whereas it did not show a significant inhibitory effect against COS-7 cells (**Fig. 7B**).

3.6 Drug-Likeness Analysis and Toxicity Prediction

The drug-likeness of 7195703 was evaluated using SwissADME. The compound fell within the optimal ranges for five physicochemical parameters (Lipophilicity, Size, Polarity, Insolubility, and Flexibility) depicted in the bioavailability radar, whereas it exceeded the acceptable range for Insaturation. 7195703 satisfied all tested drug-likeness rules, including Lipinski, Ghose, Veber, Egan, and Muegge. Furthermore, the compound was predicted to have high gastrointestinal (GI) absorption (**Fig. S5** in Online Resource 1). Regarding toxicity prediction using ProTox-3.0, the compound exhibited probabilities ranging from 0.50 to 1.0 for several toxicity endpoints (e.g., hepatotoxicity and immunotoxicity). Consequently, the predicted toxicity class was determined to be Class 4 ($300 < LD_{50}$ [mg/kg] ≤ 2000) (**Fig. S6** in Online Resource 1).

3.7 Growth Inhibitory Assay against *S. epidermidis* using Analogues

We searched for analogs of 7195703 in the ChemBridge library of approximately 1.6 million compounds to identify compounds that exhibit even stronger growth inhibitory effects, using 7195703 as a lead compound. From the SMILES in the library, we extracted compounds with a Tanimoto coefficient of 0.6 or higher, based on the Morgan fingerprint(Bajusz et al., 2015). We selected five compounds with characteristics different from those of 7195703 (**Table S4**). Then, growth inhibition assays against *S. epidermidis* were performed. However, although all five compounds showed significant growth inhibition, the maximum growth inhibition rate was 71.34% for 2274941, which did not exceed the 83.52% inhibition observed for 7195703 (**Fig. 8**). Furthermore, drug-likeness analysis and toxicity prediction were conducted for each compound using SwissADME (**Fig. S7–S11** in Online Resource 1) and ProTox-3.0 (**Fig. S12–S16** in Online Resource 1), respectively.

Discussion

The threat of drug-resistant *S. aureus* remains severe, making the development of antimicrobial agents with novel mechanisms of action an urgent priority. In this study, a hierarchical *in silico* screening combining docking simulations and MDS targeting LtaS was performed on the library of 154,118 compounds, identifying the promising candidate compound 7195703. This compound exhibited an IC_{50} value of 16.61 μM in an *in vitro* growth inhibition assay against *S. epidermidis*. This finding, combined with the 88% amino acid sequence homology between *S. epidermidis* LtaS and *S. aureus* LtaS, suggests that 7195703 is a promising drug discovery seed. Since 7195703 did not show significant growth inhibitory effects in an *in vitro* growth inhibition assay against *E. coli*, it was demonstrated that 7195703 is a compound with a narrow antimicrobial spectrum.

However, in the search for analogues of 7195703 within the library of 1,638,575 compounds, all compounds exhibited significant inhibitory effects against S. epidermidis, although no compounds surpassing the growth-inhibitory effect of 7195703 were discovered. The analog compounds possess an acetamide group at their core, enabling hydrogen bonding with ARG356. This is considered the reason why the inhibitory effect was not completely lost. Conversely, the growth inhibition rates of 2166318 (where the methoxy group of 7195703 changed to a carboxyl group) and 2302155 (where it changed to an acetamide group) decreased to 11.36% and 14.71%, respectively. This suggests that the hydrophobic interactions predicted by PLIP analysis between LEU384 and LEU413 predicted by PLIP analysis might be important for antibacterial activity. This is supported by the fact that 2274941, where the 3-chloro-4-methoxyphenyl group changed to hydrophobic naphthalene, showed the highest growth inhibition effect among the analogues. Furthermore, the activity of 2987305 and 135476455, where the 5-methoxybenzimidazole ring was altered, indicates that strict bond angles and positions are required for hydrogen bonding with TRP354. Combined with the results of binding free energy analysis using the FMO method, this suggests the importance of the hydrogen bonding.

Drug suitability analysis using SwissADME predicted that 7195703 satisfies empirical rules, including Lipinski's five rules, and possesses high GI absorption. Although weak toxicity was observed in mammalian cell assays, this compound demonstrated lower toxicity compared to the common antimicrobial agent triclosan (TCS). Moreover, it was classified as Class 4 in ProTox-3.0 predictions, suggesting its potential as a lead compound for oral administration. Notably, a correlation was observed between the Consensus Log $P_{o/w}$ (Log P) and predicted carcinogenicity among the analogues. Compounds with a Log P > 2.8 (7195703, 2274941, 2987305, 135476455) were predicted to be carcinogenic, whereas those with a Log P < 2.8 (2166318, 2302155) were not. Therefore, future drug design based on 7195703 structure should balance the maintenance of activity with safety by appropriately controlling Log P.

In future work, verifying direct antimicrobial activity through *in vitro* growth inhibition assays using clinical *S. aureus* strains, including MRSA and VRSA, is essential. Additionally, more advanced safety evaluations through *in vivo* experiments are required.

Conclusion

In this study, we conducted a hierarchical *in silico* screening targeting *S. aureus* LtaS and identified compound 7195703 as a promising hit from a library of 154,118 compounds. This compound exhibited significant growth-inhibitory activity against the model bacterium S. epidermidis, with an IC_{50} value of 16.61 mM. Furthermore, it showed no growth-inhibitory activity against *E. coli*, confirming its selectivity for Gram-positive bacteria. These results demonstrate that 7195703 represents a viable lead compound for the development of novel antimicrobial agents against *S. epidermidis* and *S. aureus*.

Statement and declaration

Acknowledgement

The authors would like to thank Mr. K. Moriyama, Mr. R. Namiguchi, and Mr. Y. Shibahara for their helpful discussions and technical assistance.

Declaration of competing interests

The authors declare that they have no conflicts of interest.

Funding

This work was supported by research funds from Kyushu Institute of Technology.

Data availability statement

The data supporting the findings of this study are available from the corresponding author upon reasonable request.

Author Contributions

Seiya Morita: Conceptualization, Methodology, Formal analysis, Investigation, Writing – original draft

Mikuri Yokota: Investigation, Formal analysis.

Kotomi Saiki: Investigation, Formal analysis.

Subaru Shioi: Investigation, Formal analysis.

Shunsuke Aoki: Conceptualization, Methodology, Resources, Writing – review and editing, Supervision, Project administration.

References

1. J.C. Lam, W. Stokes, The Golden Grapes of Wrath–Staphylococcus aureus bacteremia: A clinical review, Am J Med 136 (2023) 19–26.
2. B.P. Howden, S.G. Giulieri, T. Wong Fok Lung, S.L. Baines, L.K. Sharkey, J.Y.H. Lee, A. Hachani, I.R. Monk, T.P. Stinear, Staphylococcus aureus host interactions and adaptation, Nat Rev Microbiol 21 (2023) 380–395.
3. U. Tasneem, K. Mehmood, M. Majid, S.R. Ullah, S. Andleeb, Methicillin resistant Staphylococcus aureus: A brief review of virulence and resistance., J Pak Med Assoc 72 (2022) 509–515.
4. G. Balakirski, G. Hischebeth, J. Altengarten, D. Exner, T. Bieber, J. Dohmen, S. Engelhart, Recurrent mucocutaneous infections caused by PVL-positive Staphylococcus aureus strains: a challenge in clinical practice, JDDG: Journal Der Deutschen Dermatologischen Gesellschaft 18 (2020) 315–322. https://doi.org/10.1111/ddg.14058.

5. R.H. Deurenberg, E.E. Stobberingh, The evolution of Staphylococcus aureus, Infection, Genetics and Evolution 8 (2008) 747–763. https://doi.org/10.1016/j.meegid.2008.07.007.
6. P.D. Lyne, Structure-based virtual screening: an overview, Drug Discov Today 7 (2002) 1047–1055. https://doi.org/10.1016/S1359-6446(02)02483-2.
7. F.C. Neuhaus, J. Baddiley, A Continuum of Anionic Charge: Structures and Functions of d-Alanyl-Teichoic Acids in Gram-Positive Bacteria, Microbiology and Molecular Biology Reviews 67 (2003) 686–723. https://doi.org/10.1128/MMBR.67.4.686-723.2003.
8. A. Gründling, O. Schneewind, Synthesis of glycerol phosphate lipoteichoic acid in Staphylococcus aureus., Proc Natl Acad Sci U S A 104 (2007) 8478–83. https://doi.org/10.1073/pnas.0701821104.
9. S.G. Richter, D. Elli, H.K. Kim, A.P.A. Hendrickx, J.A. Sorg, O. Schneewind, D. Missiakas, Small molecule inhibitor of lipoteichoic acid synthesis is an antibiotic for Gram-positive bacteria., Proc Natl Acad Sci U S A 110 (2013) 3531–6. https://doi.org/10.1073/pnas.1217337110.
10. J. Taira, T. Ito, H. Nakatani, T. Umei, H. Baba, S. Kawashima, T. Maruoka, H. Komatsu, H. Sakamoto, S. Aoki, In silico structure-based drug screening of novel antimycobacterial pharmacophores by DOCK-GOLD tandem screening., Int J Mycobacteriol 6 (2017) 142–148. https://doi.org/10.4103/ijmy.ijmy_24_17.
11. Y. Koseki, T. Kinjo, M. Kobayashi, S. Aoki, Identification of novel antimycobacterial chemical agents through the in silico multi-conformational structure-based drug screening of a large-scale chemical library., Eur J Med Chem 60 (2013) 333–9. https://doi.org/10.1016/j.ejmech.2012.12.012.
12. P.T. Lang, S.R. Brozell, S. Mukherjee, E.F. Pettersen, E.C. Meng, V. Thomas, R.C. Rizzo, D.A. Case, T.L. James, I.D. Kuntz, DOCK 6: combining techniques to model RNA-small molecule complexes., RNA 15 (2009) 1219–30. https://doi.org/10.1261/rna.1563609.
13. G. Jones, P. Willett, R.C. Glen, A.R. Leach, R. Taylor, Development and validation of a genetic algorithm for flexible docking11Edited by F. E. Cohen, J Mol Biol 267 (1997) 727–748. https://doi.org/10.1006/jmbi.1996.0897.
14. O. Trott, A.J. Olson, AutoDock Vina: Improving the speed and accuracy of docking with a new scoring function, efficient optimization, and multithreading, J Comput Chem 31 (2010) 455–461. https://doi.org/10.1002/jcc.21334.
15. A. McNutt, P. Francoeur, R. Aggarwal, T. Masuda, R. Meli, M. Ragoza, J. Sunseri, D. Koes, GNINA 1.0: Molecular Docking with Deep Learning, (2021). https://doi.org/10.26434/chemrxiv.13578140.v1.
16. S. Jo, T. Kim, V.G. Iyer, W. Im, CHARMM-GUI: A web-based graphical user interface for CHARMM, J Comput Chem 29 (2008) 1859–1865. https://doi.org/10.1002/jcc.20945.
17. B.R. Brooks, C.L. Brooks III, A.D. Mackerell Jr., L. Nilsson, R.J. Petrella, B. Roux, Y. Won, G. Archontis, C. Bartels, S. Boresch, A. Caflisch, L. Caves, Q. Cui, A.R. Dinner, M. Feig, S. Fischer, J. Gao, M. Hodoscek, W. Im, K. Kuczera, T. Lazaridis, J. Ma, V. Ovchinnikov, E. Paci, R.W. Pastor, C.B. Post, J.Z. Pu, M. Schaefer, B. Tidor, R.M. Venable, H.L. Woodcock, X. Wu, W. Yang, D.M. York, M. Karplus, CHARMM: The biomolecular simulation program, J Comput Chem 30 (2009) 1545–1614. https://doi.org/10.1002/jcc.21287.

18. GROMACS Documentation Release 2022.4 GROMACS development team, 2022.
19. T. Nakano, T. Kaminuma, T. Sato, Y. Akiyama, M. Uebayasi, K. Kitaura, Fragment molecular orbital method: application to polypeptides, Chem Phys Lett 318 (2000) 614–618. https://doi.org/10.1016/S0009-2614(00)00070-1.
20. K. Kitaura, E. Ikeo, T. Asada, T. Nakano, M. Uebayasi, Fragment molecular orbital method: an approximate computational method for large molecules, Chem Phys Lett 313 (1999) 701–706. https://doi.org/10.1016/S0009-2614(99)00874-X.
21. Y. MOCHIZUKI, T. NAKANO, K. SAKAKURA, H. DOI, K. OKUWAKI, T. KATO, H. TAKIZAWA, S. OHSHIMA, T. HOSHINO, T. KATAGIRI, Current Status and Future of the ABINIT-MP Program, Journal of Computer Chemistry, Japan 23 (2024) 2024–0022. https://doi.org/10.2477/jccj.2024-0022.
22. D. Takaya, C. Watanabe, S. Nagase, K. Kamisaka, Y. Okiyama, H. Moriwaki, H. Yuki, T. Sato, N. Kurita, Y. Yagi, T. Takagi, N. Kawashita, K. Takaba, T. Ozawa, M. Takimoto-Kamimura, S. Tanaka, K. Fukuzawa, T. Honma, FMODB: The World's First Database of Quantum Mechanical Calculations for Biomacromolecules Based on the Fragment Molecular Orbital Method, J Chem Inf Model 61 (2021) 777–794. https://doi.org/10.1021/acs.jcim.0c01062.
23. N. Phusi, Y. Hashimoto, N. Otsubo, K. Imai, P. Thongdee, D. Sukchit, P. Kamsri, A. Punkvang, K. Suttisintong, P. Pungpo, N. Kurita, Structure-based drug design of novel M. tuberculosis InhA inhibitors based on fragment molecular orbital calculations, Comput Biol Med 152 (2023) 106434. https://doi.org/10.1016/j.compbiomed.2022.106434.
24. A. Daina, O. Michielin, V. Zoete, SwissADME: a free web tool to evaluate pharmacokinetics, drug-likeness and medicinal chemistry friendliness of small molecules., Sci Rep 7 (2017) 42717. https://doi.org/10.1038/srep42717.
25. P. Banerjee, E. Kemmler, M. Dunkel, R. Preissner, ProTox 3.0: a webserver for the prediction of toxicity of chemicals, Nucleic Acids Res 52 (2024) W513–W520. https://doi.org/10.1093/nar/gkae303.
26. P. Banerjee, A.O. Eckert, A.K. Schrey, R. Preissner, ProTox-II: a webserver for the prediction of toxicity of chemicals, Nucleic Acids Res 46 (2018) W257–W263. https://doi.org/10.1093/nar/gky318.
27. X. Chee Wezen, A. Chandran, R.S. Eapen, E. Waters, L. Bricio-Moreno, T. Tosi, S. Dolan, C. Millership, A. Kadioglu, A. Gründling, L.S. Itzhaki, M. Welch, T. Rahman, Structure-Based Discovery of Lipoteichoic Acid Synthase Inhibitors, J Chem Inf Model 62 (2022) 2586–2599. https://doi.org/10.1021/acs.jcim.2c00300.
28. D. Bajusz, A. Rácz, K. Héberger, Why is Tanimoto index an appropriate choice for fingerprint-based similarity calculations?, J Cheminform 7 (2015) 20. https://doi.org/10.1186/s13321-015-0069-3.
29. D. Lu, M.E. Wörmann, X. Zhang, O. Schneewind, A. Gründling, P.S. Freemont, Structure-based mechanism of lipoteichoic acid synthesis by Staphylococcus aureus LtaS, Proceedings of the National Academy of Sciences 106 (2009) 1584–1589. https://doi.org/10.1073/pnas.0809020106.

Figures

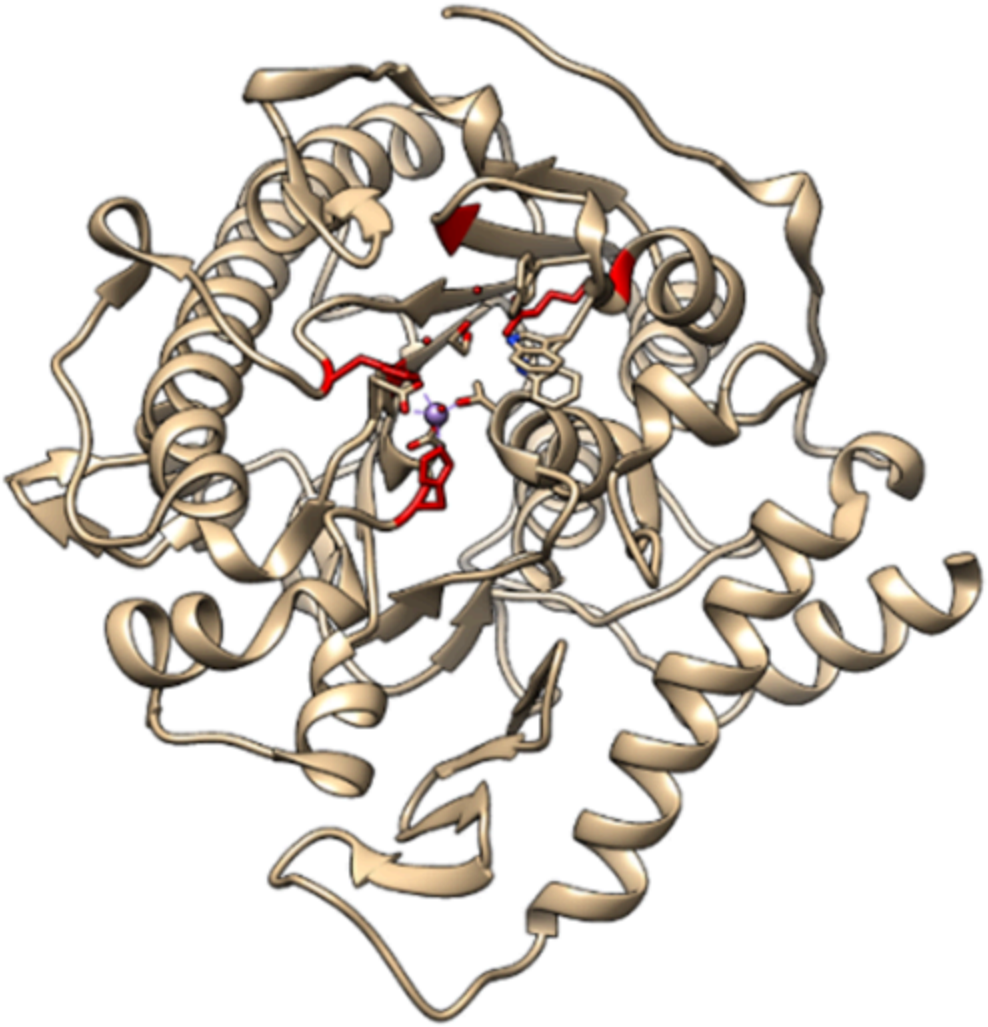


Figure 1

crystal structure of *S. aureus* eLtaS (2W5Q). Residues critical for S. aureus growth, as demonstrated in *in vitro* experiments[10], are highlighted in red. The Mn^{2+} ion is represented as a purple sphere

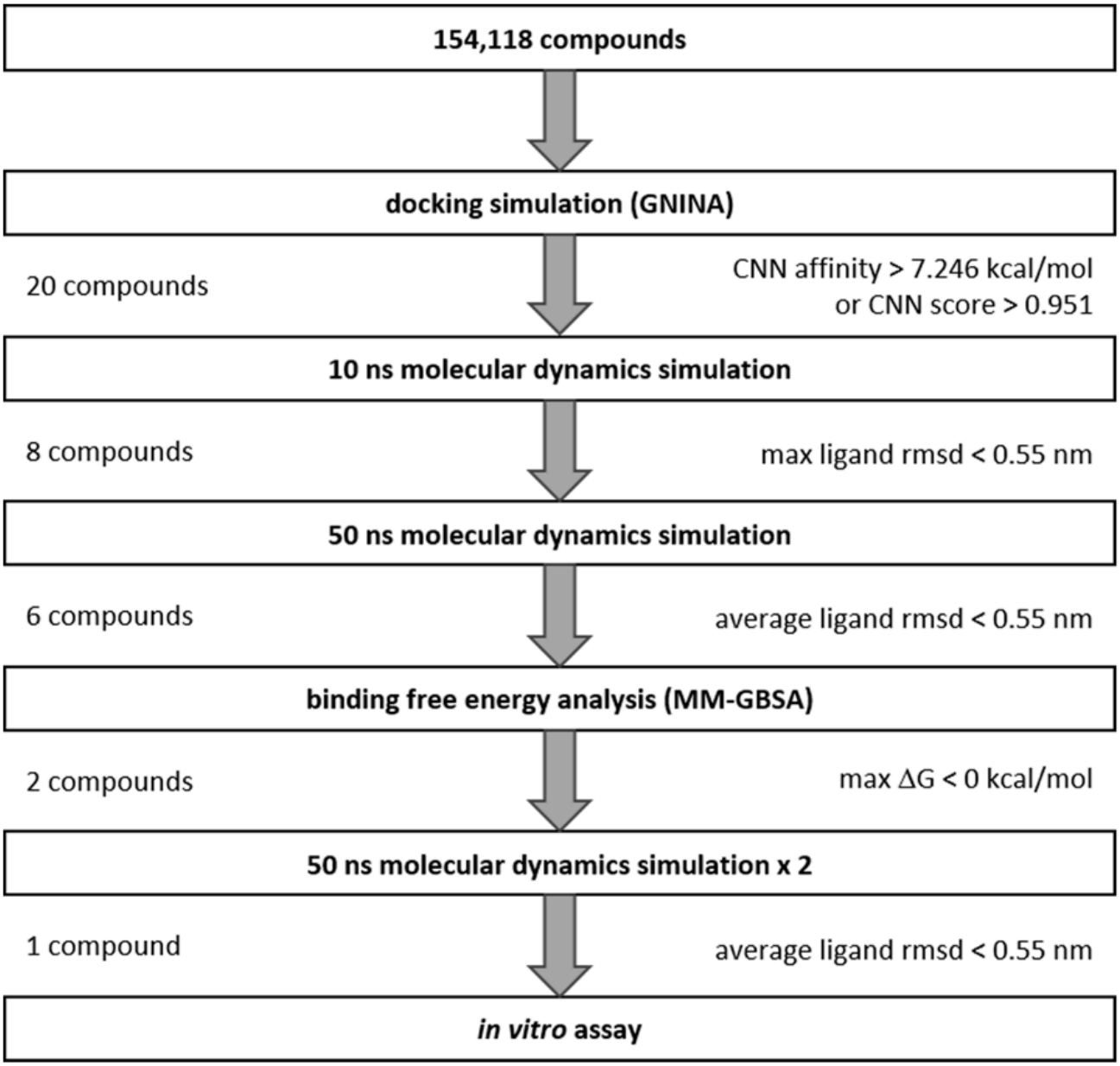


Figure 2

pathway of hierarchical *in silico* SBDS

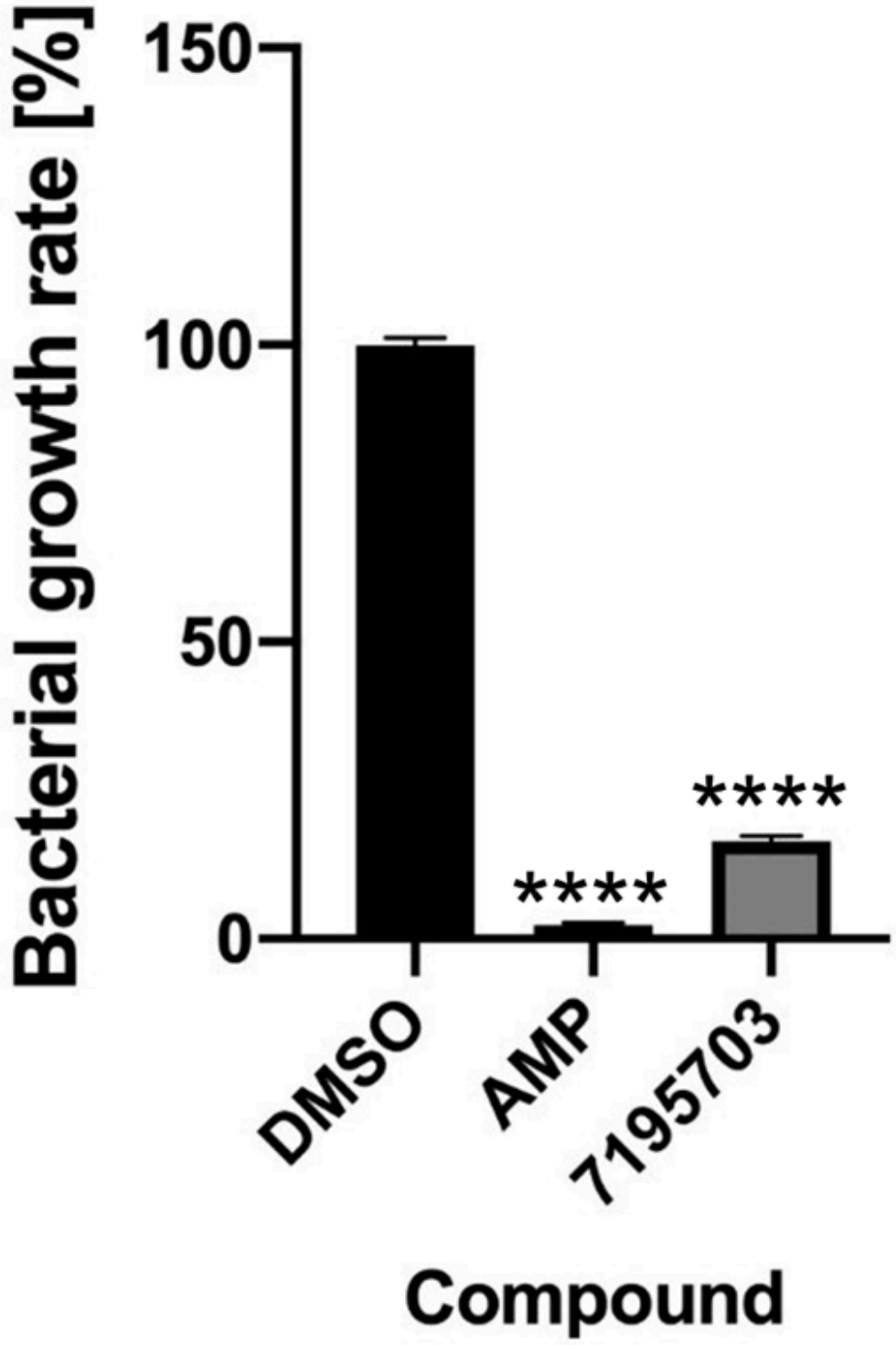


Figure 3

Inhibitory effect of 7195703 on the growth of *S. epidermidis*. Data are presented as the mean ± SEM derived from four independent experiments (n = 4). Statistical analysis was performed using Dunnett's test (****p < 0.0001)

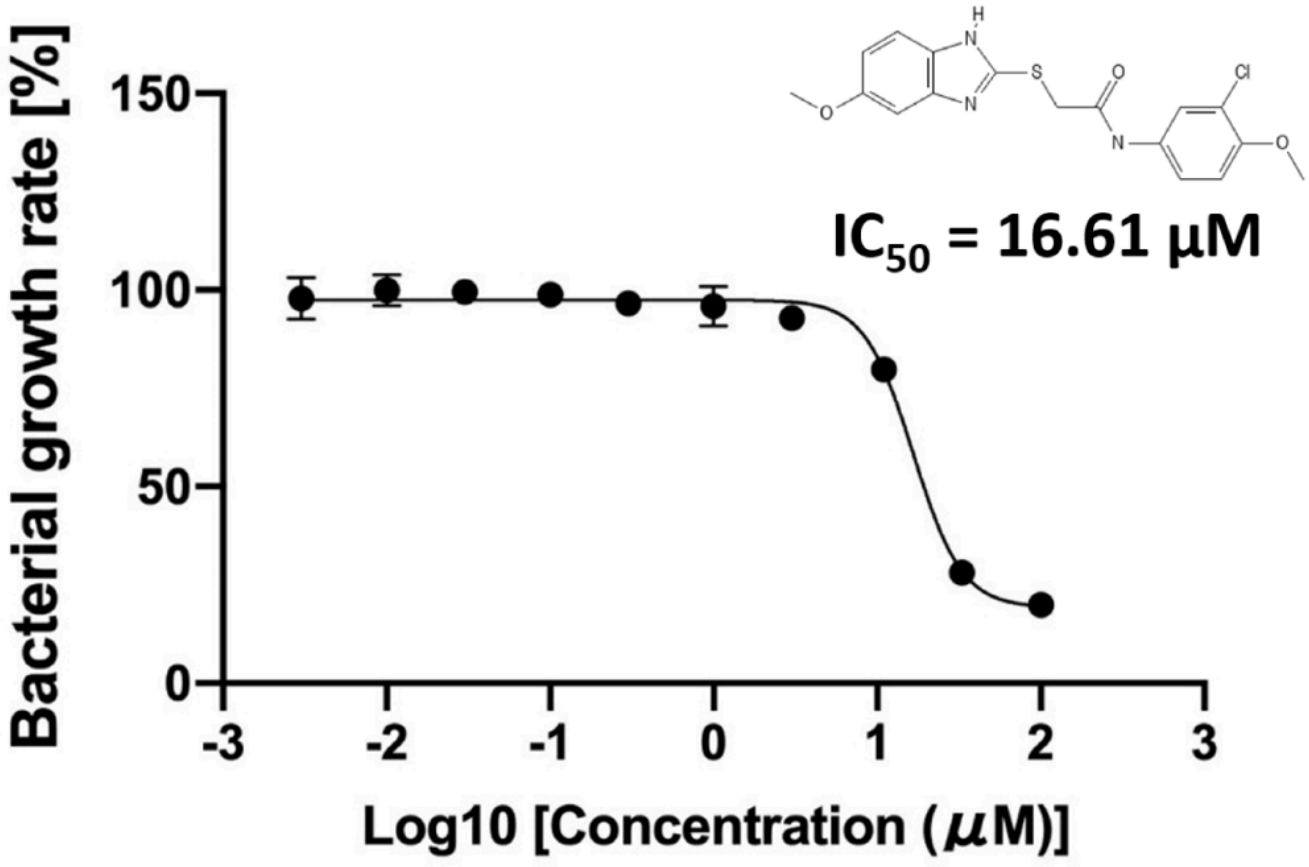
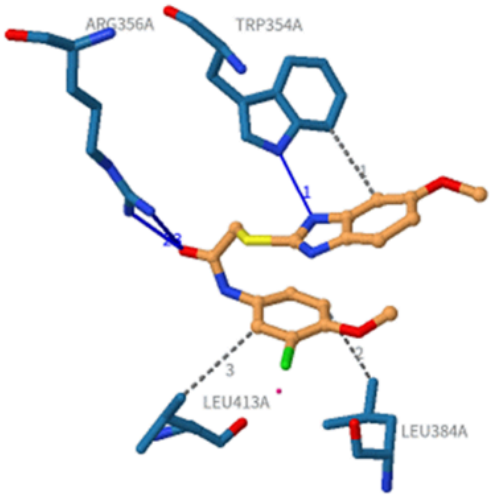


Figure 4

Dose-dependent effect of 7195703 on *S. epidermidis*. The vertical axis represents the bacterial growth rate (%) of *S. epidermidis*, and the horizontal axis represents the concentration of 7195703 on a logarithmic scale (log mM). Each plot represents the mean ± SEM of four independent experiments (n = 4). The IC_{50} value was determined using non-linear regression analysis



Hydrophobic Interactions

Index	Residue	AA	Distance	Ligand Atom	Protein Atom
1	354A	TRP	4.00	3472	1110
2	384A	LEU	3.68	3458	1369
3	413A	LEU	3.98	3461	1608

Hydrogen Bonds

Index	Residue	AA	Distance H-A	Distance D-A	Donor Angle	Protein donor?	Side chain	Donor Atom	Acceptor Atom
1	354A	TRP	2.21	2.85	120.89	×	✓	3474 [Nar]	1105 [N2]
2	356A	ARG	1.80	2.67	146.13	✓	✓	1129 [Ng+]	3455 [O2]
3	356A	ARG	3.12	3.70	118.88	✓	✓	1130 [Ng+]	3455 [O2]

Figure 5

Interaction analysis of *S. aureus* eLtaS-7195703 by the PLIP tool

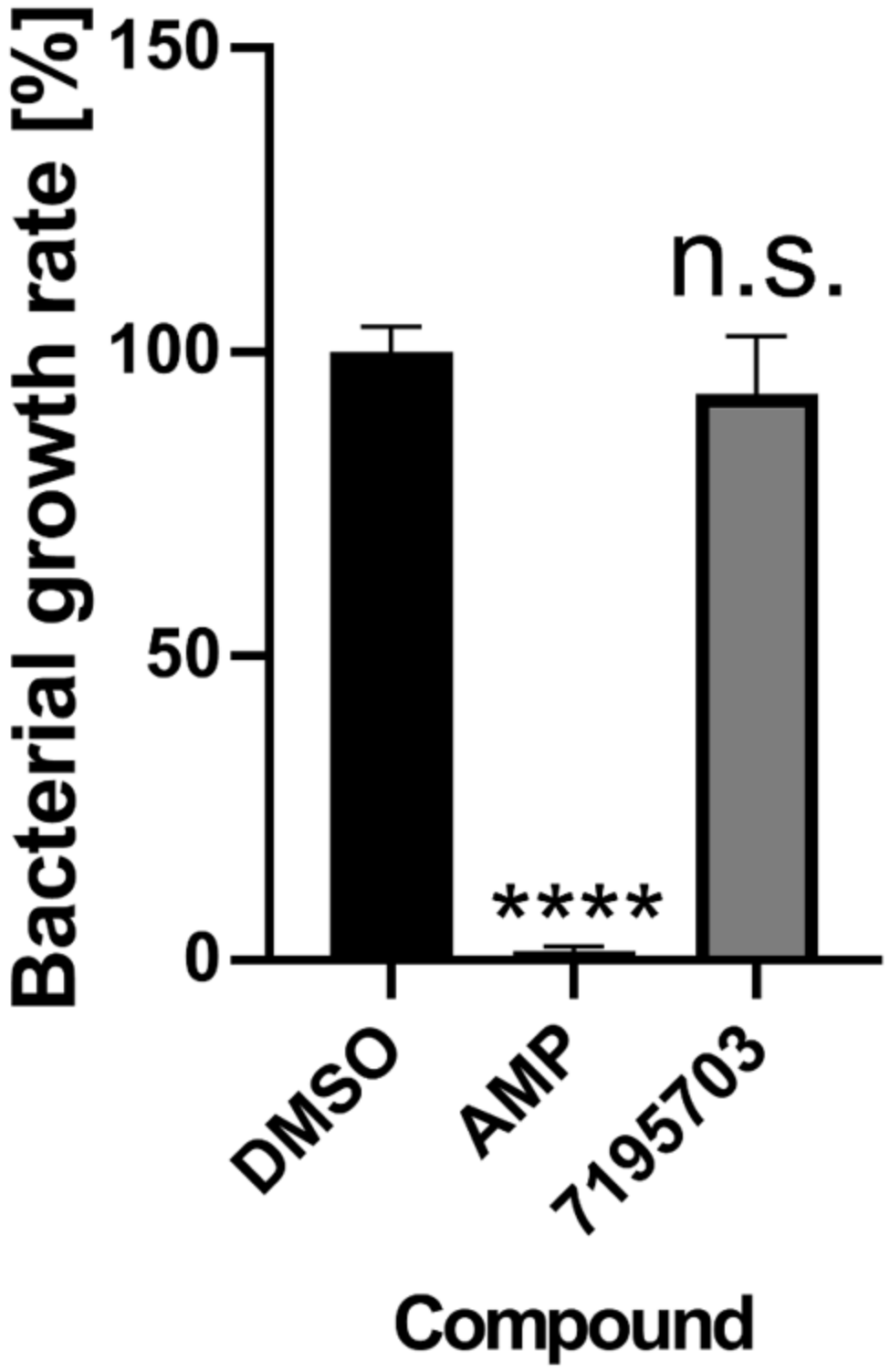


Figure 6

Inhibitory effect of 7195703 on the growth of *E. coli*. Data are presented as the mean ± SEM derived from four independent experiments (n = 4). Statistical analysis was performed using Dunnett's test (****p < 0.0001, n.s. = not significant)

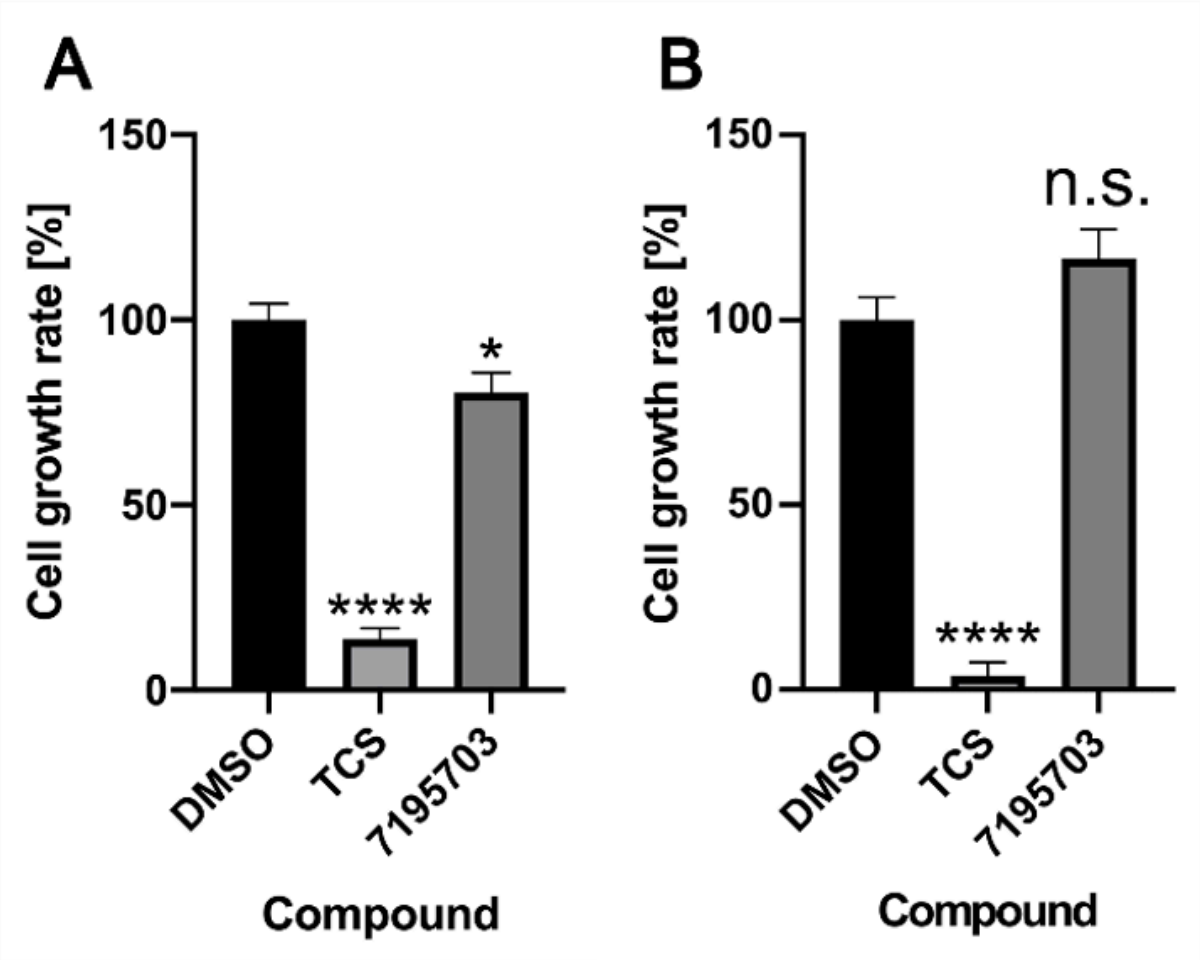


Figure 7

Effect of 7195703 on the growth of HepG2 cells (A) and COS-7 cells (B). Data are presented as the mean ± SEM derived from four independent experiments (n = 4). Statistical analysis was performed using Dunnett's test (****p < 0.0001, *p = 0.0332, n.s. = not significant)

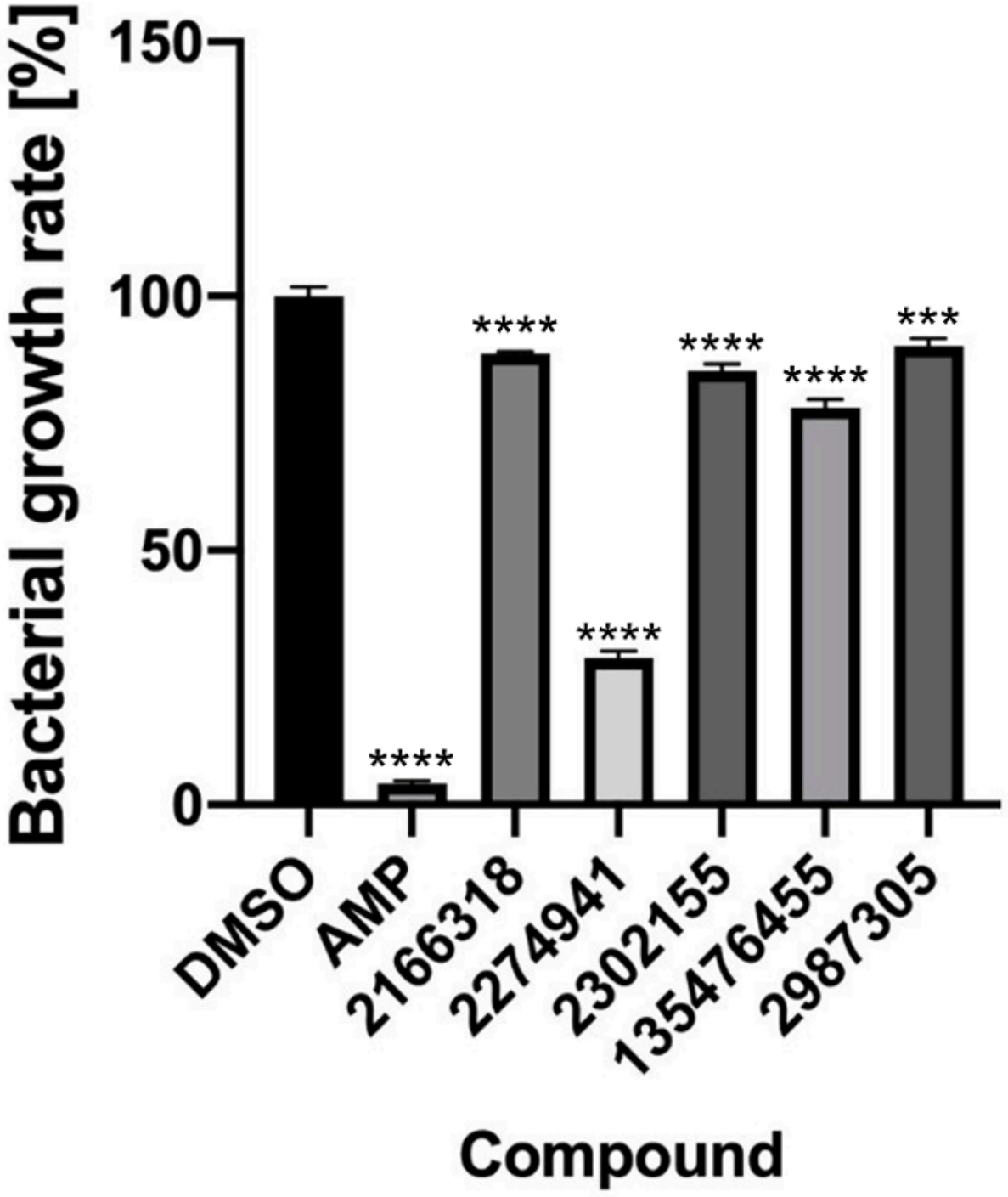


Figure 8

Inhibitory effect of analog compounds on the growth of *S. epidermidis*. Data are presented as the mean ± SEM derived from four independent experiments (n = 4). Statistical analysis was performed using Dunnett's test (****p < 0.0001, ***p = 0.0002)

Supplementary Files

This is a list of supplementary files associated with this preprint. Click to download.

- ESM1.docx